# Orange surface waveguide laser in $Pr:LiYF_4$ produced by femtosecond laser writing

AMANDINE BAILLARD,[1] PAVEL LOIKO,[1] CAROLINA ROMERO,[2] VÍCTOR ARROYO,[2] JAVIER RODRÍGUEZ VÁZQUEZ DE ALDANA,[2] MICHAËL FROMAGER,[1] ABDELMJID BENAYAD,[1] ALAIN BRAUD,[1] PATRICE CAMY,[1,*] AND XAVIER MATEOS[3]

[1]*Centre de Recherche sur les Ions, les Matériaux et la Photonique (CIMAP), UMR 6252 CEA-CNRS-ENSICAEN, Université de Caen Normandie, 6 Boulevard Maréchal Juin, 14050 Caen Cedex 4, France*
[2]*Aplicaciones del Láser y Fotónica, University of Salamanca, 37008 Salamanca, Spain*
[3] *Universitat Rovira i Virgili (URV), Física i Cristal·lografia de Materials (FiCMA), 43007 Tarragona, Spain. #Serra Húnter Fellow, Spain*
**Corresponding author: patrice.camy@ensicaen.fr*

Received XX Month XXXX; revised XX Month, XXXX; accepted XX Month XXXX; posted XX Month XXXX (Doc. ID XXXXX); published XX Month XXXX

**Depressed-cladding surface channel waveguides were inscribed in a 0.5 at.% $Pr:LiYF_4$ crystal by femtosecond Direct Laser Writing. The waveguides consisted of a half-ring cladding (inner diameter: 17 µm) and side structures ("ears") improving the mode confinement. The waveguide propagation loss was as low as 0.14±0.05 dB/cm. The orange waveguide laser operating in the fundamental mode delivered 274 mW at 604.3 nm with 28.4% slope efficiency, a laser threshold of only 29 mW and linear polarization (π), representing record-high performance for orange Pr waveguide lasers.** 

http://dx.doi.org/10.1364/OL.99.099999

Femtosecond Direct Laser Writing (fs DLW) is a powerful method to produce 3D photonic microstructures in transparent dielectric materials [1,2]. The latter absorbs the energy of fs pulses through a nonlinear process during a short time, resulting in a permanent material modification within the irradiated area (the damage track) in the µm-scale, leading to a thermally stable change of the refractive index. Laser waveguides (WGs) fabricated by this method have recently attracted significant attention [1]. The inscription of laser WGs by femtosecond pulses benefit from fast fabrication times, high precision, access to various geometries and active materials. Low to moderate propagation losses are reached for such WGs. WG lasers represent one of the building blocks of photonic integrated circuits [2]. If properly designed, they benefit from single-mode mode operation, low thresholds and high light intensities [3]. Surface WGs can be functionalized, e.g., by depositing a nonlinear optical material leading to pulsed laser operation via evanescent-field coupling [4,5].

Depending on the sign of the refractive index variation $\Delta n$ between the damage track and the surrounding unmodified (bulk) material, femtosecond laser written WGs are classified as type I ($\Delta n > 0$, guiding *within* the damage track) and type II ($\Delta n < 0$, guiding *between* the tracks) [1]. Okhrimchuk *et al.* proposed the concept of a depressed cladding WG with a core surrounded by a number of low-index damage tracks forming the cladding [6]. The tracks have a small separation, creating a quasi-continuous low-index barrier, which allows the confinement of the light. Depressed cladding WGs benefit from strong light confinement, well controlled modal profiles and low propagation losses leading to highly efficient laser operation [3]. Mode-locked WG lasers based on the depressed cladding geometry were successfully employed in high repetition rate (GHz-range) mode-locked oscillators [7,8].

So far, the majority of studies on laser waveguides elaborated by fs DLW focused on oxide crystals for emission in the near-infrared. Less studies concern fluoride matrices (glasses and crystals) [9,10]. The inscription of WGs in fluorides is more challenging because they are softer and exhibit lower refractive indices. Still, fluoride matrices can be the only viable solution to address specific laser transitions, e.g., in the visible, due to their low-phonon energy behavior and high energy position of the excited configuration $4f^{n-1}5d^1$ reducing the risk of excited-state absorption. Laser sources emitting in the visible are relevant for quantum optics, medicine and microscopy.

Praseodymium ions ($Pr^{3+}$) are known for their multi color (cyan to deep-red) emissions in the visible spectral range. Efficient and power-scalable to the watt-level output Pr bulk and fiber lasers are known [11-13]. They are based on $Pr^{3+}$-doped $LiYF_4$ crystals and ZBLAN glasses, respectively. Owing to their compact design, low laser thresholds and compatibility with the fiber technology, WG lasers can serve as seed sources for high-power fiber amplifiers. Müller *et al.* reported on the first $Pr:LiYF_4$ WG laser fabricated by fs DLW (type III geometry) [10]. Pumped by a 444-nm InGaN laser diode, the orange *channel* WG laser generated 25 mW at 604 nm with 5.6% slope efficiency and a threshold of 360 mW. Bolaños *et al.* developed low-loss (0.14 dB/cm) $Pr^{3+}$,$Gd^{3+}$,$Lu^{3+}$:$LiYF_4$ / $LiYF_4$ layers by Liquid Phase Epitaxy (LPE) [14]. Pumped by a 479 nm frequency-doubled Optically Pumped Semiconductor Laser (2ω-OPSL), the *planar* WG laser generated 165 mW at 604 nm with a slope efficiency of 32% still with a rather high threshold of 310 mW [14]. Recently, several studies focused on buried $Pr:LiYF_4$ WGs inscribed by fs laser pulses [15-18].

In the present work, we aimed to further exploit the potential of fs Direct Laser Writing for inscribing *surface channel* waveguides supporting single-transverse-mode laser operation in the visible.

Compared to planar WGs fabricated by LPE, the developed photonic microstructures benefit from strong light confinement along two orthogonal directions resulting in a nearly circular mode profile, small mode areas, notably reduced (by an order of magnitude) laser threshold, and low-loss behavior. Considering the need of further microstructuring steps for LPE-based planar WGs, ultrafast laser photoinscription represents a facile and viable route to elaborate low-loss channel WG lasers directly emitting in the visible.

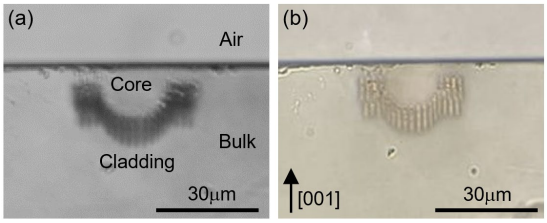


**Fig. 1.** Optical microscope images of the surface channel waveguide produced in Pr:LiYF$_4$ by fs DLW: (a) unpolarized light; (b) in crossed polarizers. [001] is the ***c***-axis.

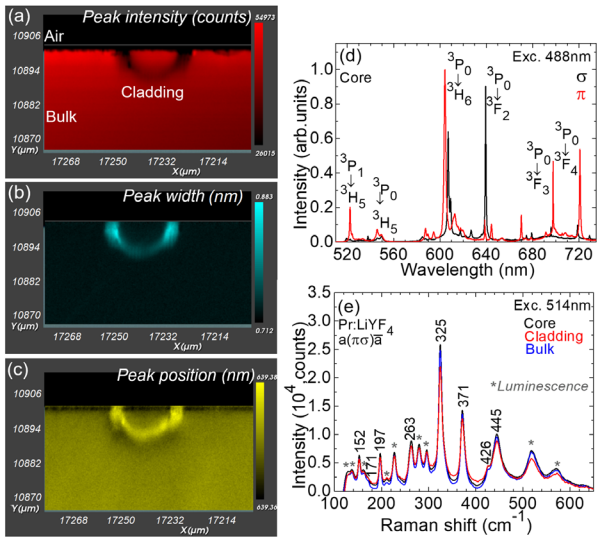


**Fig. 2.** (a-c) μ-luminescence mapping of the surface channel waveguide in Pr:LiYF$_4$ (the 639.4 nm emission peak, the $^3P_0 \rightarrow {}^3F_2$ transition): (a) peak intensity; (b) peak width; (c) peak position; (d) Luminescence spectra of $Pr^{3+}$ ions from the core region, π and σ polarizations, $\lambda_{exc}$ = 488 nm; (e) μ-Raman spectra from the core, cladding and bulk areas, ***a***(πσ)***a*** geometry, $\lambda_{exc}$ = 514 nm.

Depressed-cladding (type III) surface waveguides with a half-ring cladding were fabricated in a bulk 0.5 at.% $Pr^{3+}$:LiYF$_4$ crystal ($N_{Pr} = 0.69\times10^{20}$ at/cm$^3$) by fs DLW using 60 fs, 800 nm pulses from a Ti:Sapphire regenerative amplifier at a repetition rate of 5 kHz and a 40× objective (N.A. = 0.65). The pulse energy incident on the sample was adjusted by a λ/2 plate, neutral density filters and a linear polarizer to be 160 nJ. To produce the damage tracks, the crystal was translated in the horizontal direction (along the ***a***-axis) with a scan speed of 500 μm/s. The cladding was formed by a total of 29 damage tracks. Their horizontal separation was 2 μm. The cladding additionally contained "ears" from both sides, Fig. 1(a). The core size was 17 μm and the cladding was 30 μm-wide. The WGs were written along the entire sample length *t* of 4.5 mm. The polarization of fs radiation was parallel to the writing direction (σ). No cracks in the waveguide core nor surrounding bulk areas were observed. By placing the crystal containing the WGs between two crossed polarizers and observing it in transmission mode, an enhancement of the light intensity in the irradiated areas was revealed, Fig. 1(b), indicating stress-induced birefringence.

The μ-luminescence mapping across the sample end-facet (see [19] for details) was performed using polarized light, Fig. 2(a-d). For mapping, the emission peak in the red (at 639.4 nm, the $^3P_0 \rightarrow {}^3F_2$ transition) was selected. The integrated emission intensity, the peak width (FWHM) and the peak emission wavelength (position) were monitored over an area of 35×75 μm$^2$ with a spatial resolution of 0.5 μm. In the cladding, a decrease of emission intensity, a slight broadening of the emission peak and a red shift of its position are observed, Fig. 2(a-c). In contrast, the polarized emission properties of $Pr^{3+}$ ions in the core are well preserved with respect to the unmodified bulk regions surrounding the cladding. The same behaviour is expected for absorption of $Pr^{3+}$ ions in the WG core. μ-Raman spectroscopy reveals a broadening of the Raman peaks and a decrease of their intensity, see Fig. 2(e), which, together with the μ-luminescence findings, indicate a slight loss of crystallinity within the cladding formed by the damage tracks.

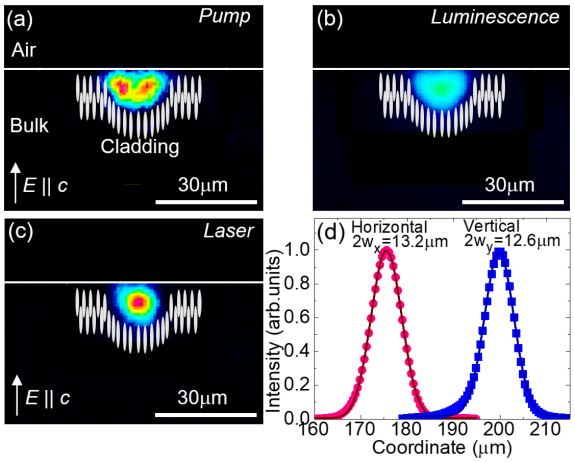


**Fig. 3.** Modal behavior of the surface channel waveguide in Pr:LiYF$_4$: (a-c) near-field mode profiles: (a) guided pump, 479.1 nm; (b) guided red luminescence; (c) laser mode, 604.3 nm. The polarization of the pump and laser emission is vertical (π); (d) 1D intensity profiles of the laser mode (*symbols*) and their Gaussian fits (*curves*) in the horizontal (*x*) and vertical (*y*) directions.

The linear laser cavity was formed by a plane pump mirror coated for high transmission (HT, $T$ = 90.2%) at 479 nm and high reflection (HR, $R$ > 99.9%) at 580-650 nm and two flat output couplers (OCs) with a transmission $T_{OC}$ of 2.5% or 12.7% at the laser wavelength (604 nm). Both bulk cavity mirrors were slightly pressed towards the WG end-facets without any index-matching liquid. The total cavity length was 4.5 mm. The crystal was mounted on a passively cooled Cu-holder using a silver paint. As a pump source, we employed a 2ω-OPSL (Genesis CX STM series, Coherent) emitting up to 1.2 W at 479.1 nm (linewidth: <0.1 nm) with $M^2 \approx 1$. The pump addressed the $^3H_4 \rightarrow {}^3P_0$ absorption band of $Pr^{3+}$ ions. The

pump polarization was adjusted using a half-wave plate to correspond to π (vertical) in the crystal. The pump beam was coupled into the WG using an antireflection (AR) coated achromatic lens (f = 40 mm) resulting in a pump spot diameter of 18±5 μm. The pump coupling efficiency was estimated from the Fresnel loss at the uncoated crystal surface. The residual (non-absorbed) pump after the OC was filtered out using a long-pass filter (FEL500, Thorlabs). The near-field modal profiles were captured using a spherical $CaF_2$ lens (f = 15 mm) and a CCD-camera (BladeCam2-XHR, DataRay). The laser emission spectra were measured by an optical spectrum analyzer (AQ6373B, Yokogawa) with a resolution of 0.02 nm.

The near-field modal profiles of the guided pump radiation, guided red luminescence and orange laser emission are shown in Fig. 3(a-c). The white ellipses indicate the damage tracks forming the cladding. The waveguide is multimode for the pump radiation. Both the pump and laser modes are well confined within the cladding. The 1D intensity profiles of the laser mode are well fitted with a Gaussian distribution. The laser mode is nearly circular, with the measured beam diameters at the $1/e^2$ level of 13.2($x$) × 12.6($y$) μm², see Fig. 3(d) where $x$ and $y$ refer to the horizontal and vertical ($||\boldsymbol{c}$) directions. The intensity profile of the laser mode in the vertical direction is slightly asymmetric.

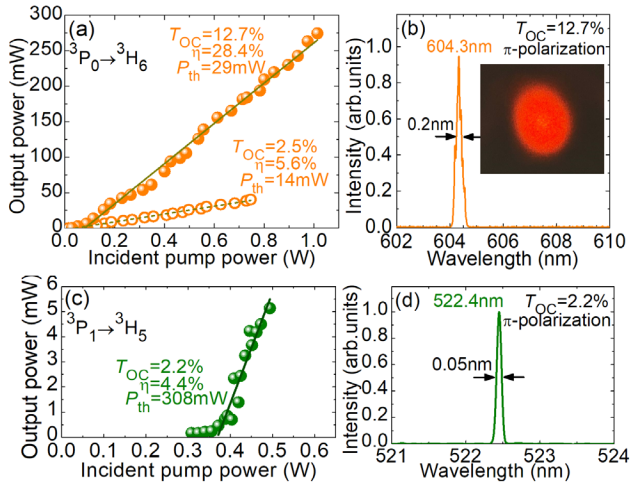


**Fig. 4.** Pr:$LiYF_4$ surface channel waveguide lasers: (a,b) Orange laser, the $^3P_0 \rightarrow {}^3H_6$ transition; (c,d) Green laser, the $^3P_1 \rightarrow {}^3H_5$ transition: (a,c) input-output dependences, $\eta$ – slope efficiency, $P_{th}$ – laser threshold; (b,d) spectra of laser emission, π-polarization. *Inset* – photograph of the orange laser beam in the far-field.

The surface waveguide laser in Pr:$LiYF_4$ generated a maximum output power of 274 mW at 604.3 nm with a slope efficiency $\eta$ of 28.4% (vs. the incident pump power) and a low laser threshold of 29 mW (for high output coupling of 12.7%), Fig. 4(a). The optical efficiency at the maximum incident pump power of 1.0 W reached 27.1%. The output dependence was linear and further power scaling was limited by the available pump. For smaller $T_{OC}$ of 2.5%, the laser threshold was further reduced to 14 mW at the expense of lower output power (40 mW) and slope efficiency ($\eta$ = 5.6%). For this OC, the pump power was limited to 0.75 W due to the higher intracavity laser intensity. No damage of the WG end-facets nor laser mirrors was observed. The observed very low laser thresholds are related to a strong light confinement and small mode areas in the inscribed surface WG, as well as the four-level laser scheme for the $^3P_0 \rightarrow {}^3H_6$ $Pr^{3+}$ transition.

A typical spectrum of the orange laser emission is given in Fig. 4(b). The laser linewidth (FWHM) was 0.2 nm. The polarization state of the laser emission was studied using a Glan-Taylor polarizer, see Fig. 5. The laser emission was linearly polarized, and the polarization state (π, vertical) was naturally selected by the anisotropy of the gain, cf. Fig. 2(d). Laser emission in the red was not observed despite the high emission cross-section for the $^3P_0 \rightarrow {}^3F_2$ transition for σ-polarization due to much higher WG propagation losses, as well as poor mode confinement for light polarized along the horizontal axis ($\boldsymbol{E} \perp \boldsymbol{c}$, σ). A photograph of the orange laser beam on a black screen in the far-field is shown at the inset of Fig. 4(b). It shows a slight beam ellipticity due to its stronger divergence along the vertical direction. The beam quality factors $M^2_{xy}$ were measured by an ISO-standard method yielding values below 1.3. This, together with the Gaussian intensity profiles of the near-field laser mode, confirms single-transverse-mode operation of the orange WG laser.

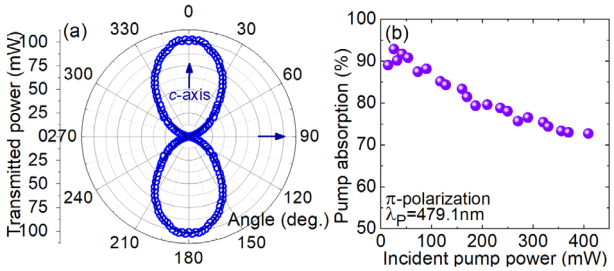


**Fig. 5.** (a) Analysis of the polarization state of the orange Pr:$LiYF_4$ laser, $T_{OC}$ = 12.7%, $P_{inc}$ = 0.45 W; (b) Measured single-pass pump absorption in the WG (non-lasing conditions).

The divergence of the output beam along the horizontal direction ($\theta$, half-angle) was measured to be 0.030. Using the approximation of a step-index waveguide, $N.A.^2 \approx 2n_{core}\Delta n$, where N.A. = $\sin\theta$, we estimated the variation of the refractive index in the damage tracks forming the cladding $\Delta n$ as $-3\times10^{-4}$ (the extraordinary refractive index of $LiYF_4$ $n_{core}(e)$ is 1.4760 at 604 nm).

The pump absorption efficiency (for single-pass pumping) in the waveguide under non-lasing conditions was determined in a pump-transmission measurement, see Fig. 5(b). For comparison, we also calculated the small-signal absorption, $\eta_{abs,0} = 1 - \exp(-\sigma_{abs}N_{Pr}t)$, which amounted to >99%, using the absorption cross-section $\sigma_{abs}$ of $17\times10^{-20}$ $cm^2$ for π-polarization. A significant absorption saturation was observed. Assuming that the inversion population is clamped at the threshold pump power, for the orange WG laser, we obtained $\eta_{abs,L}$ = 92.4%, so that the laser slope efficiency vs. the absorbed pump power was 32.0% and the laser threshold – 26 mW.

The waveguide propagation loss at the laser wavelength was estimated by simulating the laser performance with a model of a four-level laser yielding 0.14±0.05 dB/cm.

So far, laser action from Pr:$LiYF_4$ WGs fabricated by fs DLW was achieved in the orange, red and deep-red spectral ranges. We also targeted the transition in the green ($^3P_1 \rightarrow {}^3H_5$). We used a pump mirror providing a transmission $T$ = 59.8% at the pump wavelength and HR ($R$ > 99.9%) at 520 nm, and an OC with $T_{OC}$ of 2.2% at 520 nm. To suppress the high-gain orange laser line, both mirrors provided higher transmission at 604 nm ($T_{PM}$ = 15.8% and $T_{OC}$ = 64.1%). The green laser delivered 5.1 mW at 522.4 nm (laser

linewidth: 0.05 nm) with a slope efficiency of 4.4% and a high laser threshold of 308 mW, see Fig. 4(c,d). The laser emission was linearly polarized (π). For the green WG laser, $\eta_{abs,L}$ = 75.5% and the laser slope efficiency thus reached 6.1%.

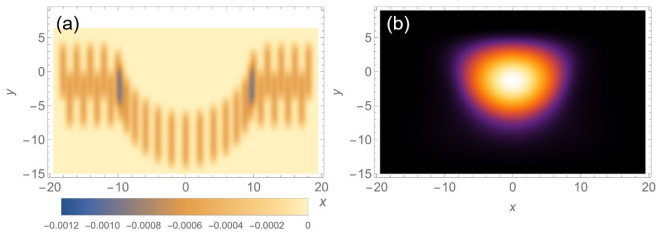


**Fig. 6.** Simulation of the (a) spatial distribution of the refractive index variation and (b) fundamental mode for the surface channel waveguide in Pr:$LiYF_4$ (π-polarization).

Numerical simulations of the modal profile were performed by solving the 2D wave equation with the imaginary-distance beam propagation method [20]. The wave equation was discretized in a cartesian grid with a step of 0.15 μm. The refractive index decrease obtained from the N.A. estimation was used. The spatial distribution of the refractive index variation and the simulated fundamental mode (π-polarized light) are shown in Fig. 6. The modal profile has an asymmetric shape along the vertical axis due to the surface boundary, and symmetric shape in the horizontal direction. The confinement along the *x*-axis is good due to the extra tracks added at the sides of the waveguide ("ears"), contributing to a decreased leakage out of the waveguide further decreasing the propagation losses. The obtained modal profile is similar to the guided red luminescence, Fig. 3(b), and slightly differs from the laser mode, Fig. 3(c). The additional spatial mode filtering effect for the orange laser may originate from the weak $^3H_4 \rightarrow {}^1D_2$ reabsorption [11].

Compared to the previous results on orange Pr:$LiYF_4$ waveguide lasers fabricated by both LPE and fs DLW, cf. Table 1, we report on the record-high output power and laser slope efficiency, as well as the lowest laser threshold. This work also represents the first demonstration of a *surface* Pr:$LiYF_4$ channel WG laser. The achieved laser performance is due to a combination of (i) a small mode area in the fabricated WG, (ii) very low propagation losses and (iii) the use of high-brightness pumping. We also report on the first lasing in the green from a fs DLW waveguide laser in Pr:$LiYF_4$.

**Table 1. Output Characteristics of Orange Pr:$LiYF_4$ Waveguide Lasers Reported So Far**

| Method | $\lambda_{pump}$, nm | $P_{th}$, mW | $P_{out}$, mW | $\delta_{loss}$, dB/cm | $\eta$, % | Ref. |
|---|---|---|---|---|---|---|
| Fs DLW | $444^{LD}$ | 360 | 25 | 2.3 | $5.6^{Inc}$ | [10] |
| | $444^{LD}$ | 100 | 86 | 0.12 | $16^{Coupl}$ | [15] |
| | $444^{LD}$ | 120 | 121 | 0.12 | $16.6^{Inc}$ | [16] |
| | $479.1^{OPSL}$ | **29** | **274** | 0.14 | $28.4^{Inc}$ | This work |
| LPE | $479.2^{OPSL}$ | 305 | 165 | 0.14 | $32^{Abs}$ | [14] |

To conclude, depressed-cladding surface waveguides with optimized writing parameters and cladding design including side structures ("ears") fabricated in bulk $Pr^{3+}$:$LiYF_4$ crystals by fs Direct Laser Writing enable low propagation losses (0.14 dB/cm at 604 nm) and single-mode laser operation in the orange. As revealed by μ-Raman and μ-luminescence studies, the anisotropic emission properties of $Pr^{3+}$ ions in the WG core are well preserved. We report on the record-high output power from any orange Pr WG laser, as well as the lowest laser threshold from such a device. We also achieved laser action in the green from a femtosecond laser written Pr:$LiYF_4$ waveguide laser. The developed WGs are promising for surface functionalization, e.g., by graphene or carbon nanotubes for pulsed laser operation via evanescent field coupling. It is promising to test other $Pr^{3+}$-doped laser crystals (including oxide ones) for ultrafast laser inscription of WGs.

**Funding.** Agence Nationale de la Recherche (ANR-22-CE08-0025-01, NOVELA); Contrat de plan État-Région (CPER) de Normandie. Grant PID2019-108543RB-I00 funded by MCIN/AEI/10.13039/501100011033.

**Disclosures.** The authors declare no conflicts of interest.

**Data availability.** Data underlying the results presented in this paper are not publicly available at this time but may be obtained from the authors upon reasonable request.

## References

1. F. Chen and J. R. V. de Aldana, Laser Photonics Rev. **8**, 251 (2014).
2. G. D. Marshall, A. Politi, J. C. F. Matthews, P. Dekker, M. Ams, M. J. Withford, and J. L. O'Brien, Opt. Express **17**, 12546 (2009).
3. E. Kifle, P. Loiko, C. Romero, J. R. V. de Aldana, M. Aguiló, F. Díaz, P. Camy, U. Griebner, V. Petrov, and X. Mateos, Progr. Quantum Electron. **72**, 100266 (2020).
4. E. Kifle, P. Loiko, J. R. V. de Aldana, A. Ródenas, S. Y. Choi, F. Rotermund, V. Zakharov, A. Veniaminov, M. Aguiló, F. Díaz, U. Griebner, V. Petrov, and X. Mateos, Photonics Res. **6**, 971 (2018).
5. Y. Tan, C. Cheng, S. Akhmadaliev, S. Zhou, and F. Chen, Opt. Express **22**, 9101 (2014).
6. A. G. Okhrimchuk, A. V. Shestakov, I. Khrushchev, and J. Mitchell, Opt. Lett. **30**, 2248 (2005).
7. A. G. Okhrimchuk and P. A. Obraztsov, Sci. Rep. **5**, 11172 (2015).
8. S. Y. Choi, T. Calmano, F. Rotermund, and C. Kränkel, Opt. Express **26**, 5140 (2018).
9. D. G. Lancaster, S. Gross, A. Fuerbach, H. E. Heidepriem, T. M. Monro, and M. J. Withford, Opt. Express **20**, 27503 (2012).
10. S. Müller, T. Calmano, P. Metz, N.-O. Hansen, C. Kränkel, and G. Huber, Opt. Lett. **37**, 5223 (2012).
11. C. Kränkel, D.-T. Marzahl, F. Moglia, G. Huber, and P. W. Metz, Laser Photonics Rev. **10**, 548 (2016).
12. E. Kifle, F. Starecki, P. Loiko, S. Cozic, F. Joulain, T. Berthelot, T. Georges, D. Stojcevski, D. Deubel, and P. Camy, Opt. Lett. **46**, 74 (2021).
13. M. Xiong, Y. Zhao, D. Wang, Z. Chen, B. Xu, A. Nizamutdinov, V. Semashko, and S. Korableva, Opt. Lett. **48**, 4725 (2023).
14. W. Bolaños, G. Brasse, F. Starecki, A. Braud, J.-L. Doualan, R. Moncorgé, and P. Camy, Opt. Lett. **39**, 4450 (2014).
15. D. Baiocco, I. Lopez-Quintas, J. R. V. de Aldana, M. Tonelli, and A. Tredicucci, Opt. Lett. **48**, 1734 (2023).
16. Y. Ren, Z. Cui, L. Sun, C. Wang, H. Liu, and Y. Cai, Chin. Opt. Lett. **20**, 122201 (2022).
17. H. Liu, S. Luo, B. Xu, H. Xu, Z. Cai, M. Hong, and P. Wu, Opt. Mater. Express **7**, 3990 (2017).
18. D. Beckmann, D. Esser, and J. Gottmann, Appl. Phys. B **104**, 619 (2011).
19. E. Kifle, P. Loiko, X. Mateos, J. R. Vázquez de Aldana, A. Ródenas, U. Griebner, V. Petrov, M. Aguiló, and F. Díaz, Opt. Mater. Express **7**, 4258 (2017).
20. Y. Tsuji and M. Koshiba, J. Light. Technol. **18**, 618 (2000).

## Full references


1. F. Chen and J. R. V. de Aldana, "Optical waveguides in crystalline dielectric materials produced by femtosecond-laser micromachining," Laser Photonics Rev. **8**(2), 251-275 (2014).
2. G. D. Marshall, A. Politi, J. C. F. Matthews, P. Dekker, M. Ams, M. J. Withford, and J. L. O'Brien, "Laser written waveguide photonic quantum circuits," Opt. Express **17**(15), 12546-12554 (2009).
3. E. Kifle, P. Loiko, C. Romero, J. R. V. de Aldana, M. Aguiló, F. Díaz, P. Camy, U. Griebner, V. Petrov, and X. Mateos, "Watt-level ultrafast laser inscribed Thulium waveguide lasers," Progr. Quantum Electron. **72**, 100266 (2020).
4. E. Kifle, P. Loiko, J. R. V. de Aldana, A. Ródenas, S. Y. Choi, F. Rotermund, V. Zakharov, A. Veniaminov, M. Aguiló, F. Díaz, U. Griebner, V. Petrov, and X. Mateos, "Passively Q-switched fs-laser-written thulium waveguide laser based on evanescent field interaction with carbon nanotubes," Photonics Res. **6**(10), 971-980 (2018).
5. Y. Tan, C. Cheng, S. Akhmadaliev, S. Zhou, and F. Chen, "Nd:YAG waveguide laser Q-switched by evanescent-field interaction with graphene," Opt. Express **22**(8), 9101-9106 (2014).
6. A. G. Okhrimchuk, A. V. Shestakov, I. Khrushchev, and J. Mitchell, "Depressed cladding, buried waveguide laser formed in a YAG:$Nd^{3+}$ crystal by femtosecond laser writing," Opt. Lett. **30**(17), 2248-2250 (2005).
7. A. G. Okhrimchuk and P. A. Obraztsov, "11-GHz waveguide Nd:YAG laser CW mode-locked with single-layer graphene," Sci. Rep. **5**(1), 11172 (2015).
8. S. Y. Choi, T. Calmano, F. Rotermund, and C. Kränkel, "2-GHz carbon nanotube mode-locked Yb:YAG channel waveguide laser," Opt. Express **26**(5), 5140-5145 (2018).
9. D. G. Lancaster, S. Gross, A. Fuerbach, H. E. Heidepriem, T. M. Monro, and M. J. Withford, "Versatile large-mode-area femtosecond laser-written Tm:ZBLAN glass chip lasers," Opt. Express **20**(25), 27503-27509 (2012).
10. S. Müller, T. Calmano, P. Metz, N.-O. Hansen, C. Kränkel, and G. Huber, "Femtosecond-laser-written diode-pumped Pr:$LiYF_4$ waveguide laser," Opt. Lett. **37**(24), 5223-5225 (2012).
11. C. Kränkel, D.-T. Marzahl, F. Moglia, G. Huber, and P. W. Metz, "Out of the blue: semiconductor laser pumped visible rare-earth doped lasers," Laser Photonics Rev. **10**(4), 548-568 (2016).
12. E. Kifle, F. Starecki, P. Loiko, S. Cozic, F. Joulain, T. Berthelot, T. Georges, D. Stojcevski, D. Deubel, and P. Camy, "Watt-level visible laser in double-clad $Pr^{3+}$-doped fluoride fiber pumped by a GaN diode," Opt. Lett. **46**(1), 74-77 (2021).
13. M. Xiong, Y. Zhao, D. Wang, Z. Chen, B. Xu, A. Nizamutdinov, V. Semashko, and S. Korableva, "Watt-level and near diffraction-limited $Pr^{3+}$-doped single-crystal fiber lasers," Opt. Lett. **48**(18), 4725-4728 (2023).
14. W. Bolaños, G. Brasse, F. Starecki, A. Braud, J.-L. Doualan, R. Moncorgé, and P. Camy, "Green, orange, and red $Pr^{3+}$:$YLiF_4$ epitaxial waveguide lasers," Opt. Lett. **39**(15), 4450-4453 (2014).
15. D. Baiocco, I. Lopez-Quintas, J. R. V. de Aldana, M. Tonelli, and A. Tredicucci, "Diode-pumped visible lasing in femtosecond-laser-written Pr:$LiLuF_4$ waveguide " Opt. Lett. **48**(7), 1734-1737 (2023).
16. Y. Ren, Z. Cui, L. Sun, C. Wang, H. Liu, and Y. Cai, "Laser emission from low-loss cladding waveguides in Pr:YLF by femtosecond laser helical inscription," Chin. Opt. Lett. **20**(12), 122201 (2022).
17. H. Liu, S. Luo, B. Xu, H. Xu, Z. Cai, M. Hong, and P. Wu, "Femtosecond-laser micromachined Pr:YLF depressed cladding waveguide: Raman, fluorescence, and laser performance," Opt. Mater. Express **7**(11), 3990-3997 (2017).
18. D. Beckmann, D. Esser, and J. Gottmann, "Characterization of channel waveguides in Pr:$YLiF_4$ crystals fabricated by direct femtosecond laser writing," Appl. Phys. B **104**, 619-624 (2011).
19. E. Kifle, P. Loiko, X. Mateos, J. R. Vázquez de Aldana, A. Ródenas, U. Griebner, V. Petrov, M. Aguiló, and F. Díaz, "Femtosecond-laser-written hexagonal cladding waveguide in Tm:$KLu(WO_4)_2$: μ-Raman study and laser operation," Opt. Mater. Express **7**(12), 4258-4268 (2017).
20. Y. Tsuji and M. Koshiba, "Guided-mode and leaky-mode analysis by imaginary distance beam propagation method based on finite element scheme," J. Light. Technol. **18**(4), 618 (2000).